

1 **TITLE**

2 ***Bartonella henselae* Persistence within Mesenchymal Stromal Cells Enhances Endothelial**
3 **Cells Activation and Infectability Amplifying the Angiogenic Process.**

4

5 **Scutera Sara^{1*} Mitola Stefania^{2*} Sparti Rosaria¹ Salvi Valentina² Grillo Elisabetta² Piersigilli**

6 **Giorgia¹ Bugatti Mattia² Alotto Daniela³ Schioppa Tiziana^{2,4} Sozzani Silvano^{5*} Musso**

7 **Tiziana^{1#*}**

8 * Contributed equally

9 # Corresponding author

10 **Affiliations**

11 ¹Department of Public Health and Pediatric Sciences, University of Torino, Italy.

12 ²Department of Molecular and Translational Medicine, University of Brescia, Italy.

13 ³Skin Bank, Department of General and Specialized Surgery, A.O.U. Città della Salute e della
14 Scienza, Turin, Italy.

15 ⁴Humanitas Clinical and Research Center-IRCCS Rozzano-Milano, Italy.

16 ⁵Laboratory Affiliated to Istituto Pasteur Italia-Fondazione Cenci Bolognetti, Department of
17 Molecular Medicine, Sapienza University of Rome, Italy.

18 **Correspondence**

19 Tiziana Musso tiziana.musso@unito.it

20

21

22

23

24

25

26

27 **ABSTRACT**

28 Some bacterial pathogens can manipulate the angiogenic response, suppressing or inducing it for
29 their own ends. In humans, *B. henselae* is associated with cat-scratch disease and
30 vasculoproliferative disorders such as bacillary angiomatosis and bacillary peliosis. Although
31 endothelial cells (ECs) support the pathogenesis of *Bartonella*, the mechanisms by which
32 *Bartonella* induces EC activation are not completely clear, as well as the possible contribution of
33 other cells recruited at the site of infection. Mesenchymal stromal cells (MSCs) are endowed with
34 angiogenic potential and play a dual role in infections exerting antimicrobial properties but also
35 acting as a shelter for pathogens.

36 Here we delved into the role of MSCs as reservoir of *Bartonella* and modulator of EC functions. *B.*
37 *henselae* readily infected MSCs and survived in perinuclear bound vacuoles for up to 8 days.
38 Infection enhanced MSC proliferation and the expression of EGFR, TLR2 and NOD1, proteins that
39 are involved in bacterial internalization and cytokine production. Secretome analysis revealed that
40 infected MSCs secreted higher levels of the proangiogenic factors VEGF, FGF-7, MMP-9, PIGF,
41 serpin E1, TSP-1, uPA, IL-6, PDGF-D, CCL5 and CXCL8. Supernatants from *B. henselae*-infected
42 MSCs increased the susceptibility of ECs to *B. henselae* infection and enhanced EC proliferation,
43 invasion and reorganization in tube-like structures.

44 Altogether, these results candidate MSCs as a still underestimated niche for *B. henselae* persistent
45 infection and reveal a MSC-EC crosstalk that may contribute to exacerbate bacterial-induced
46 angiogenesis and granuloma formation.

47

48 **KEYWORDS**

49 Mesenchymal stromal cells, *B. henselae*, angiogenesis, VEGF, CXCL8, EGFR, TLR, NOD

50

51

52

53

54 **INTRODUCTION**

55 Endemic among domestic cats, *B. henselae* is a fastidious gram-negative bacterium that, in humans,
56 can cause subclinical intraerythrocytic bacteremia, mainly transmitted by cat fleas. In
57 immunocompetent individuals, *B. henselae* infection can also lead to cat-scratch disease (CSD),
58 characterized by lymphadenopathy with suppurative granulomas. Atypical clinical presentations of
59 CSD, ranging from prolonged fever of unknown origin to hepatosplenic, ocular and neurological
60 manifestations, have also been reported (1).

61 Individuals unable to mount an immune response against *B. henselae* tend to develop a
62 tumor-like vascular proliferative response in the skin and/or internal organs, which can lead to
63 bacillary angiomatosis (BA) or bacillary peliosis (BP) (2). After infection, *B. henselae* survives,
64 stimulates the migration and the production of pro-angiogenic factors by human endothelial cells
65 (ECs) (2–5). In addition, other cells types, such as monocytes/macrophages (6), recruited to the
66 vasoproliferative lesions, stimulate EC proliferation in a paracrine manner through the production
67 of VEGF and CXCL8 (7). Mononuclear phagocytes, CD34⁺ progenitor cells and ECs can also
68 function as a reservoir from which *B. henselae* periodically enters the bloodstream and disseminates
69 within the host (8). Despite the clinical implications of protracted *Bartonella* infections, the
70 underlying mechanism of intracellular *B. henselae* persistence is poorly understood, and the
71 existence of different reservoirs still remains to be determined.

72 Mesenchymal stem cells (MSCs) are multipotent adult stem cells present in various tissues,
73 including the bone marrow and the adipose tissue, which have recently received much attention due
74 to their regenerative potential and immunomodulatory properties (9). MSCs actively participate in
75 angiogenesis through several mechanisms, including paracrine cytokines and exosomes and cell
76 contact interactions with endothelial cells. (10, 11). A diverse and multitasking role of MSCs during
77 bacterial infection has recently emerged (12, 13). MSCs can sense pathogens and mount an
78 appropriate cytokine/chemokine response through the activation of Toll-like receptors (TLRs),

79 NOD-like receptors (NLRs) and the scavenger receptors MARCO and SR-B1 (12). Moreover,
80 MSCs express EGFR, a (member of the ErbB receptor tyrosine kinase family), shown to enhance
81 their proliferation and the release of angiogenic factors (14). However, despite the emerging role of
82 MSCs in infectious diseases, the mechanisms regulating the interplay between MSCs and bacteria
83 are yet to be defined. Recent evidence suggests that MSCs can have a double edge sword effect by
84 playing a role in clearing infection but also promoting persistent bacterial infection. MSCs exert
85 antimicrobial effects by secreting antimicrobial peptides and expressing indoleamine2,3-
86 dioxygenase (IDO) and MSC administration reduce pathogen burden in animal models of
87 antimicrobial sepsis (12). However, MSCs can also serve as a niche where *M. tuberculosis* can
88 survive and persist during antimicrobial therapy. Indeed, viable *M. tuberculosis* was recovered from
89 MSCs infiltrating TB granulomas in humans and in a tuberculosis mouse model (15, 16). It is likely
90 that other chronic bacterial pathogens may exploit MSCs to favor their survival in the host and we
91 hypothesized that *B. henselae* infects MSCs and that infected-MSCs contribute to the angiogenesis
92 via interaction with endothelial cells that are one of *Bartonella* preferential target.
93 Here we show that *B. henselae* can invade and survive within human MSCs and demonstrate that
94 TLR2, NOD1 and EGFR are implicated in bacterial recognition and cytokine production.
95 Moreover, we provides evidence for a MSC-EC crosstalk involved in bacteria intracellular survival
96 and activation of a proangiogenic program.

97

98

99 RESULTS

100 ***B. henselae* invades and persists in MSCs.** To characterize the interaction of MSCs with
101 *B. henselae*, adipose-derived MSCs were infected with MOI of 100:1 for 1, 2, 3, 4 and 8 days and
102 then treated with gentamicin to kill all residual extracellular bacteria. Subsequently, the number of
103 viable intracellular bacteria was measured by colony-forming unit (CFU) assay. The number of *B.*

104 *henselae* invading MSCs increased progressively over a 3-day period and the number of CFUs in
105 MSCs remained unchanged up to 8 days ($P < 0.05$) (Fig. 1a). At day 8 post-infection (pi), the vast
106 majority of MSCs contained *B. henselae*, as demonstrated by the strong cytoplasmic reactivity of an
107 anti-*B. henselae* monoclonal antibody (anti-BH) (Fig. 1b, upper panel). The presence of internalized
108 bacteria was confirmed by immunofluorescence (Fig. 1B, lower panel). To assess *B. henselae*
109 intracellular survival after the initial infection and gentamicin treatment, MSCs were cultured in
110 medium without gentamicin for four additional days. The number of viable intracellular bacteria
111 recovered, which remained stable during the first 96 h, was significantly lower at day 8 compared to
112 day 4 (Fig. 1c). The ability of *B. henselae* to invade MSCs was further assessed by comparing its
113 infection efficiency in MSCs vs HUVECs, a known target of *B. henselae* infection. The number of
114 intracellular bacteria recovered after 24 h of infection from MSCs was significantly higher than that
115 recovered from HUVECs (Fig. 1d).

116 Next, we followed MSC infection by fluorescence microscopy. At day 1 pi, *B. henselae*
117 stained with DAPI (Cyan) remained mainly anchored to the MSC membrane, with only a few
118 bacteria present in the cytoplasm (Fig. 2a, upper right panel, arrowhead). From day 2 pi onward, the
119 number of internalized bacteria increased, and most of *B. henselae* were enclosed in perinuclear
120 vesicles (Fig. 2a, lower left and central panel, thin arrows). After 8 days pi, aggregates of bacteria
121 colocalized with F-actin in globular structures called invasomes, first described in *Bartonella*-
122 infected ECs (Fig. 2a, lower right panel, large arrow; and Fig. 2b) as attested by 3D
123 immunofluorescence analysis.

124 Altogether, these findings indicate that *B. henselae* is internalized by MSCs, even more
125 efficiently than HUVECs, where it can persist for a prolonged time.

126 ***B. henselae* infection enhances MSC proliferation.** We next asked whether *B. henselae*
127 infection would affect MSC survival. *B. henselae* infection did not induce cell death in MSCs as
128 demonstrated by similar amounts of Annexin V positive cells found in uninfected vs infected MSCs

129 (Fig. 3a). This finding was further supported by the unaltered *Bcl-2* (antiapoptotic) /*Bax* (apoptotic)
130 expression ratio observed in these cells (Fig. 3b). We then assessed the effect of infection on the
131 proliferation rate of MSCs. Infected-MSCs grew significantly faster compared to their uninfected
132 counterparts. Conversely, heat-inactivated *B. henselae* (HK *B. henselae*) failed to enhance MSC
133 proliferation (Fig. 3c).

134 **Role of TLR2, EGFR and NOD1 in MSC infection with *B. henselae*.** TLRs and NODs
135 play a key role in bacterial detection and their cooperation become relevant in the context of
136 infections. Interaction between cell surface TLR2 and intracellular surveillance NOD1/2 are of
137 relevance in the recognition of pathogens and in the induction of the inflammatory response (17).
138 However a number of cell surface receptors, such EGFR, that signal through pathways not related
139 to TLRs and NODs, are also used by pathogens and an interaction between TLRs and EGFR has
140 been demonstrated (18, 19).

141 We therefore assessed the expression of these receptors in response to *B. henselae* infection.
142 Interestingly, *B. henselae* infection led to a more than 6-fold increase in TLR2 expression at both
143 mRNA and protein levels, while TLR4 expression remained basically unchanged (Fig. 4a and 4b).
144 Furthermore, RT-PCR analysis showed a significant upregulation of NOD1 mRNA at day 2 and 4
145 pi (Fig. 4a). NOD2 gene expression was not detected in uninfected or infected MSCs. Lastly, *B.*
146 *henselae* infection significantly increased EGFR mRNA and phosphorylation levels (Fig. 4a and 4c,
147 respectively). Specifically, we detected increased phosphorylation as early as 30 min pi, which
148 remained above basal levels up to 120 min pi (Figure 4c).

149 The involvement of these receptors was evaluated in the production of CXCL8, a cytokine
150 shown to be triggered by *Bartonella* in different cell types (20), *Bartonella* infection of MSCs
151 enhanced their ability to produce CXCL8, which was neutralized by incubation with an anti-TLR2
152 neutralizing antibody (Fig. 4d, upper panel). Similarly, treatment with the EGFR inhibitor gefitinib
153 or with the selective RIP2K inhibitor GSK583 significantly reduced the release of CXCL8 in *B.*
154 *henselae*-infected MSCs (Fig. 4d, lower panel), suggesting that the EGFR/NOD pathway may play

155 a role in CXCL8 transcriptional regulation. Finally, to address the role of bacterium-activated
156 EGFR in *Bartonella* entry, we treated MSCs with the EGFR inhibitor gefitinib and a neutralizing
157 anti-EGFR antibody, detecting a reduced bacterial internalization by about 70% and 50%,
158 respectively, compared to untreated cells (Fig. 4e).

159 ***B. henselae*-infected MSCs promote angiogenesis and infection of endothelial cells.**

160 Since MSCs regulate vascular remodeling and angiogenesis (21), we assessed the proangiogenic
161 activity of conditioned medium (CM) from *B. henselae*-infected MSCs. To this end, CM from
162 uninfected or *B. henselae*-infected MSC cultures were tested in a scratch wound healing assay using
163 HUVECs. CM from *B. henselae*-infected MSCs (CM-MSC *B. henselae*), induced a more rapid
164 repair of HUVECs monolayer (Fig. 5a). In addition, the CM-MSC *B. henselae* was 9 fold more
165 powerful than CM of uninfected MSC (CM-MSC CTRL) on aspheroid-based sprouting assay,
166 which faithfully recapitulate the proliferation, invasion and reorganization in tube-like structure of
167 ECs (Fig. 5b). In keeping with the proangiogenic activity of MSCs, the CM-MSC CTRL induced
168 the formation of radial sprouts, similarly to what induced by spheroids stimulation with 30 ng/mL
169 of VEGF-A (Fig. 5b, right panel). Importantly, CM-MSC *B. henselae* but not that from uninfected
170 cells (CM-MSC CTRL) accelerated the morphogenesis of HUVECs when seeded on Cultrex
171 Extracellular Matrix, as judged by the number of closed structures formed at 18 h pi (Fig. 5c).

172 Even though ECs and MSCs can crosstalk through soluble mediators (22), there is no data
173 on the effects of MSC on the susceptibility of ECs to bacterial infection. We thus assessed the
174 extent of *Bartonella* internalization, at day 1 pi, in HUVECs pretreated with CM from uninfected
175 MSCs (CM-MSC CTRL) or *B. henselae*-infected MSCs (CM-MSC *B. henselae*). While there were
176 no differences in the yield of bacteria between control HUVECs (Ctrl) and HUVECs pretreated
177 with CM-MSC CTRL, a significantly higher number of bacteria was detected in HUVECs
178 pretreated with CM-MSC *B. henselae* (Fig. 5d). After 1 day of culture we did not observe a
179 significant increase in the proliferation of infected HUVECs pre-treated with CM-MSC *B. henselae*
180 over that pre-treated with CM-MSC CTRL, or directly infected. The number of cells

181 harvested/number of cells seeded (mean \pm SEM) obtained were 1.23 ± 0.2 (unconditioned medium),
182 1.063 ± 0.06 (*B. henselae* infected), 1.125 ± 0.1 (CM-MS CTR) and 1.25 ± 0.05 (CM-MS *B.*
183 *henselae*). In accord with our observation endothelial cell proliferation during *B. henselae* infection
184 has been shown after 3 or 4 days of incubation (7, 23). Our results indicate that the treatment with
185 CM-MS *B. henselae* makes HUVECs more infectable and the increase in intracellular CFU does
186 not depend on HUVEC proliferation.

187 **Angiogenic expression profile of *B. henselae*-infected MSCs.** Finally, we assessed the
188 impact of *B. henselae* infection on the ability of MSCs to modulate the expression of
189 proinflammatory and proangiogenic molecules. For this purpose, we probed an antibody
190 angiogenesis array with CM from uninfected and 4-day-infected MSCs. Among the 55 proteins of
191 the assay, 27 were detected in CM of both uninfected and infected MSCs. Densitometric analysis
192 showed the upregulation of FGF-7, CXCL8, MMP-9, PIGF, Serpin E1, TSP-1, uPA and VEGF, in
193 *B. henselae*-infected MSCs CM compared to those from uninfected MSCs (Fig. 6a and 6b).
194 Intriguingly, activin A was the only growth factor downregulated in *B. henselae*-infected MSCs
195 (Fig. 6a and 6b). Of note, the elevated expression of MCP-1, PTX3 and TIMP-1 was not modulated
196 by infection (Fig. 6a, and 6b). The quantification by ELISA of the increased production of CXCL8
197 and VEGF in the supernatants of MSCs infected for 1, 4 and 7 days was in good agreement with the
198 array data (Fig. 6c). Finally, other molecular factors known for their angiogenic activity, but not
199 included in our array, such as IL-6, CCL5 and PDGF-D, were also induced following *B. henselae*
200 infection (Fig. 6c).

201 DISCUSSION

202 *Bartonella* spp exploits several mechanisms to hide inside erythrocytes and ECs to evade
203 immune responses and persist in both animal reservoir and human host. Numerous evidence
204 indicate that the blood-stage phase is preceded by the infection of cellular niches that periodically
205 release bacteria able to invade erythrocytes. ECs were the first cell types considered a primary niche
206 as they support *Bartonella* replication and reside in proximity to the bloodstream (2, 24). However,

207 later studies identified additional *Bartonella* persistence sites including hematopoietic progenitor
208 cells and dendritic cells (8, 25).

209 Here we show that once inside, *B. henselae* resides in MSCs without proliferating for
210 several days. During this time, *Bartonella* localizes in numerous perinuclear membrane bound
211 vacuoles, as previously shown in HUVECs and MonoMac cells (26, 27), or at late time points of
212 infection, as aggregated bacteria enclosed into F actin-rich cell membrane protrusions identified as
213 invasome structures (28).

214 MSCs sense microorganisms through the expression of various PRR including Toll-like
215 receptors (TLRs) and Nod-like receptors (NLRs). The engagement of such receptors modulate MSC
216 functions and their abilities to secrete cytokines (29). Our studies revealed that TLR2, NOD1 and
217 EGFR are involved in the recognition and responses to *Bartonella* by MSCs. Upon infection with
218 *B. henselae*, MSCs secrete large amounts of CXCL8, which is curbed by incubation with an anti-
219 TLR2 antibody. A central role of TLR2 signaling during *Bartonella* infection is consistent with
220 previous findings indicating that *B. henselae*, despite being Gram-negative, preferentially activates
221 TLR2 (25). In infected cells, NOD1 and NOD2 recognize bacterial peptidoglycan derivatives
222 released into the cytosol and, upon ligand association with the adaptor protein receptor-interacting-
223 serine/threonine-protein kinase 2 (RIPK2 or RIP2), trigger proinflammatory signaling (30). In our
224 experimental system, inhibition of the RIP2 with the highly RIPK2-specific compound
225 GSK583(31) decreased CXCL8 release, indicating that NOD1 activation and signaling through
226 RIP2 during MSC infection is, in part, responsible for inducing the inflammatory response to *B.*
227 *henselae* infection. Consistent with our results, NOD1 mediates CXCL8 induction after recognition
228 of *Helicobacter pylori*, *Escherichia coli* (32, 33) and *Chlamydia pneumoniae* (34). Importantly,
229 gefitinib, an inhibitor of EGFR tyrosine kinase domain, used to treat various forms of cancer, can
230 hamper *B. henselae*-mediated induction of CXCL8, suggesting a role of EGFR in this pathway.
231 Gefitinib also exerts an off-target inhibitory activity on the expression of RIP2 (35), thus the
232 inhibition of CXCL8 secretion may be due to blockage of NOD/RIP2 signaling alongside that of

233 EGFR. In support to this hypothesis, EGFR/NOD cooperation has been recently involved in
234 cytokine production in dengue virus infected monocytes (36). Moreover, a growing body of
235 literature highlights the importance of EGFR/ErbB in several bacterial and viral inflammatory
236 responses (18, 37) and in pathogenic angiogenesis (38). In addition to stimulation of EGFR tyrosine
237 phosphorylation, *Bartonella* enhanced EGFR mRNA expression suggesting that this upregulation
238 could serve as a positive feedback system. A functional role of EGFR signaling in the immune
239 response against *B. henselae* is further supported by the observation that treatment of MSCs with
240 the kinase inhibitor gefitinib or an anti-EGFR antibody significantly decreases *Bartonella*
241 internalization. In this regard, EGFR has been recently shown to act as a cofactor in mediating
242 pathogen internalization in host cells (e.g., HBV, HCV, Chlamydia and Candida) (18). Our finding
243 indicates an important role of EGFR activation in *Bartonella* invasion; however, as these EGFR
244 inhibitors do not completely abrogate *Bartonella* uptake by MSCs, it is likely that other receptors,
245 other than EGFR, may play a role in *Bartonella* infection. Moreover, it remains to be investigated
246 whether EGFR activation is due to the direct interaction of *Bartonella* with the EGFR extracellular
247 domain or by its transactivation by EGFR ligands (i.e., EGF, HBEGF, TGF α , BTC, AREG, EREG
248 and EPGN) as shown for *H. pylori* and *Neisseria* spp. (39, 40). EGFR signaling pathways exert an
249 antiapoptotic activity in *Pseudomonas*- and *Helicobacter*- infected cells (41, 42) suggesting that
250 EGFR activation by *Bartonella* promotes the survival and proliferation of infected MSCs.

251 These effects may also be explained at least in part by the robust release of cytokine/growth
252 factors caused by *Bartonella* infection. In addition to CXCL8, angiogenic factors upregulated in
253 infected MSCs include FGF-7, MMP-9, PIGF, serpin E1, TSP-1, uPA, IL-6, CCL5 and VEGF,
254 leading to the induction of a proangiogenic phenotype in ECs as well as an increased susceptibility
255 of ECs to infection. Data reporting a role of MSCs in facilitating the infection of other cell types are
256 sparse and concern mainly phagocytic cells. MSCs was shown to enhance bacterial uptake and
257 clearance by PMNs (43), and to mediate the reactivation of HIV in monocytic cells (44). A
258 secretome highly rich in inflammatory angiogenic cytokines and matrix remodeling factors was

259 previously described in *B. henselae* infected myeloid angiogenic cells (MACs). Similarly to our
260 observation in MSCs conditioned medium from MACs increased angiogenic sprouting (45). In the
261 past, infected ECs have been shown to upregulate the expression of VEGF and CXCL8 that
262 directly lead to host cell proliferation and potentiate angiogenesis (23, 46); in parallel, *Bartonella*
263 triggers the release of proinflammatory chemokines which recruit monocytes/macrophages in the
264 vasoproliferative lesions and the production of angiogenic factors by phagocytic cells upon
265 infection plays a central role in mediating angiogenesis-(7, 20, 45). Since at sites of
266 infection/inflammation, MSCs localize in contact with ECs (22, 47), we propose that infected
267 MSCs may support this angiogenic loop.

268 A role for MSCs can be envisioned in different scenarios of *Bartonella* infections. For
269 instance, MSCs are recruited in tuberculosis around the lymph node granulomas to establish a
270 persistent infection and likely to suppress T cell response (48). Moreover, MSCs are found in oral
271 pyogenic granuloma tissues (49). Granulomatous lymphadenitis is the pathological hallmark of cat
272 scratch disease whereby MSCs could also be hired in *Bartonella* granuloma to contribute to the
273 immune pathogenesis. MSCs reside in the bone marrow (BM) interacting with other cellular
274 components. We have previously shown the co-localization DCs and MSCs in human BM (50). The
275 role of MSC-EC crosstalk has been characterized in the maintenance of the hematopoietic stem cell
276 niche and in infection-induced emergency myelopoiesis (51, 52). Interestingly MSCs were shown to
277 regulate proliferation and erythroid differentiation of CD34⁺ stem cells (53). As *B. henselae* can
278 infect CD34⁺ BM progenitor cells, BM has been proposed as one of the potential niches. In this
279 regard, multifocal BM involvement was shown in CSD (54, 55) and a contribution of *B. henselae* to
280 ineffective erythropoiesis was suggested (56). *Bartonella*-infected MSCs, releasing soluble
281 molecules, can recruit and activate ECs which in turn collaborate with MSCs in the fine regulation
282 of the hematopoietic stem cell niche.

283 In conclusion, this study provides novel insights into the role of MSCs in serving as a
284 reservoir during *B. henselae* infection and identifies TLR2, NOD1 and EGFR as the receptors

285 involved in the recognition of *B. henselae*. Infection of MSCs triggers a potent proangiogenic
286 program, which activates and enhances EC susceptibility to bacterial infection. A better
287 understanding of the involvement of MSCs in *Bartonella*-induced angiogenesis may allow the
288 development of targeted therapeutic strategies for the treatment of vascular proliferative disorders.

289 MATERIALS AND METHODS

290

291 **Cell culture.** Human MSCs were isolated from adipose tissues as previously described (50).
292 Human adipose tissues were collected by lipoaspiration from healthy donors after written consent
293 and in compliance with the Declaration of Helsinki and the local Ethic Committee (Comitato Etico
294 Interaziendale A.O.U. Città della Salute e della Scienza di Torino - A.O. Ordine Mauriziano - ASL
295 TO1, No. 0009806). Subsequently, MSCs were analyzed by flow cytometry to verify their
296 phenotype was positive for CD73, CD90 and CD105 and negative for CD11b, CD34 and CD45.

297 HUVECs were isolated from umbilical cords of healthy informed volunteers in compliance
298 with the Declaration of Helsinki. HUVECs were used at early (I-IV) passages and grown on culture
299 plates coated with porcine gelatin in M199 medium (Gibco Life Technologies, ThermoFisher
300 Scientific Group) supplemented with 20% heat-inactivated fetal calf serum (FCS, Gibco Life
301 Technologies), endothelial cell growth factor (ECGF) (10 µg/mL), and porcine heparin (100
302 µg/mL) (Sigma Aldrich) (100 µg/mL) or in complete EBM2 medium (Lonza Group Ltd Basel,
303 Switzerland).

304 **Bacterial cultures.** *B. henselae* Houston I strain (ATCC 49882; Manassas, VA, USA) was
305 grown on 5% sheep blood Columbia agar plates (BioMerieux, Lyon, France) under anaerobic
306 conditions (i.e., candle jar) at 37°C for 10 days. Bacteria were harvested under a laminar-flow hood
307 by gently scraping colonies off the agar surface. They were then suspended in MICROBANK™
308 cryopreservative solution and stored at -80°C in 1-mL aliquots. For biological assays, frozen
309 bacteria were incubated in Schneider's Insect Medium (Sigma-Aldrich) supplemented with 10%
310 FBS, as described by Riess et al (57), at 37°C and 5% CO₂ for 6 days. Spectrophotometry was

311 performed to evaluate bacterial growth [optical density (OD₆₀₀) 0.6, corresponding to 1x10⁸
312 bacteria/mL] and confirmed by plating serial dilutions on 5% sheep blood Columbia agar plates.
313 Bacteria, washed 3 times with 1X PBS, were then added to cell cultures. Where indicated, *B.*
314 *henselae* were killed by heating thawed bacteria at 56°C for 30 min.

315 **Preparation of conditioned medium.** MSCs, cultured into 12-well plates at a density of
316 0.5×10^5 cells/well in RPMI 10% FBS without antibiotics, were left untreated or infected for 96 h
317 with *B. henselae*. Cells were then extensively washed to remove extracellular bacteria, and fresh
318 RPMI was replaced for 72 h. Conditioned medium was collected, centrifuged at 4000 rpmi for 10
319 min and then filtered, aliquoted, and stored at -20°C.

320 **Infection assay.** *B. henselae* invasion of MSCs was assessed by GPA. Briefly, 12,500
321 cells/cm² MSCs were seeded for 24 h in RPMI supplemented with 10% FCS. To compare MSCs
322 with HUVECs, infection was carried out with 60,000 cells *per* well seeded in DMEM 10% FCS or
323 complete EBM2 medium (Lonza Group Ltd), respectively. The next day, cells were washed twice
324 and cultured in RPMI supplemented with 10% FCS without antibiotics. *B. henselae* (MOI 100) was
325 added to the cells, immediately centrifuged at 1200 g for 5 min to allow the association of bacteria
326 with the cellular surface, and incubated for 1, 2, 3, 4 and 8 days. At the end of infection period,
327 gentamicin sulfate (Sigma-Aldrich) (100 µg/mL) was added to the medium for 2 h to kill all
328 extracellular bacteria. This assay was performed in triplicate, and control wells were left uninfected.
329 Cells were then washed extensively and lysed by the addition of 200 µL of distilled water for 5 min
330 and sonicated for 1.30 min. Lysates were serially diluted, plated on Columbia blood agar, and CFUs
331 were counted after 1 week of incubation. To determine intracellular survival after 96 h of infection,
332 extracellular bacteria were killed by gentamicin treatment for 2 h. Cells were further incubated in
333 normal medium for the remaining time of the indicated infection period. When indicated, cells were
334 pretreated for 6 h with the specific inhibitors gefitinib (10 µM) and GSK583 (1 µM) (both from
335 MedChemExpress NJ, USA) or with a specific antibody against EGFR (mouse IgG1, clone LA1) or
336 its corresponding isotype control antibody (both from EMD Millipore Corporation CA, USA) at 10

337 $\mu\text{g/ml}$. GPA was performed as described above after 1 or 2 days. In some experiments, HUVECs
338 were cultured in the presence of CM from untreated and infected MSCs. Briefly cells seeded at
339 60,000 cells per well were pretreated overnight with the indicated CM and then infected with *B.*
340 *henselae* (MOI 100) for 24 h. Cells were harvested and counted directly with an hemacytometer.
341 Proliferation is reported as an index calculated as number of cells harvested/number of cells seeded.
342 In parallel a GPA assay was performed.

343 **Staining procedures.** MSCs (1×10^4) were seeded on glass coverslips and infected with *B.*
344 *henselae* at a MOI of 100. For immunohistochemical staining, cells were fixed in methanol,
345 saturated with 0.1% BSA in PBS and incubated for 1h with an anti-*B. henselae* mAb (anti-BH,
346 dilution 1:50, mouse IgG2b/clone H2A10, Abcam, Cambridge, United Kingdom). The H2A10
347 clone reacts with a 43-kDa epitope present only in *B. henselae* strains and not in other Bartonella
348 species (58). After washing an anti-mouse biotinylated Ab was added for 30 min. and the slides
349 were then stained with horseradish peroxidase streptavidin (HRP Streptavidin) or with the
350 chromogen DAB (3, 3'-diaminobenzidine) (ThermoFisher Scientific). For immunofluorescence
351 analysis, the slides were incubated with anti-BH mAb, followed by goat anti-mouse Alexa Fluor®
352 594 (dilution 1:500, A21023, ThermoFisher Scientific). Nuclei were counterstained with DAPI
353 (4',6-diamidin-2-fenilindolo) (ThermoFisher Scientific). To follow bacterial infection, MSCs were
354 seeded at 0.25×10^4 on glass coverslips, infected with *B. henselae* (MOI 100) and incubated for 1, 2,
355 3, 4 and 8 days. At the end of infection period, cells were fixed with 4% paraformaldehyde (PFA)
356 for 10', washed with PBS and permeabilized in PBS with 0.25% saponin. Samples were then
357 saturated with blocking solution (PBS with 5% normal goat serum, and 2% BSA) for 1h at RT.
358 After washes in PBS, samples were incubated with the wheat germ agglutinin-Alexa Fluor 594 or
359 488 conjugate, Alexa Fluor® 594 phalloidin (A12381) (1 h) and with DAPI (5 min) (all from
360 ThermoFisher Scientific CA, USA) to stain cell membranes, actin and nuclei/bacteria respectively.
361 Cells were analyzed under a Zeiss Observer.Z1 epifluorescence microscope equipped with a Plan-
362 Apochromat 100 \times /1.4 NA oil objective and ApoTome2 imaging system for optical sectioning. Z-

363 stack images were elaborated through AxioVision 3D and Extended Focus modules.

364 **Immunoblotting.** Total cell lysates from cells untreated or treated for 30, 60 and 120 min
365 with *B. henselae* (MOI 100) or with 50 ng/ml EGF (R&D System, MN, USA) for 15 min, were
366 prepared in cold lysis buffer (1% Triton X-100, 1% NP-40 in PBS, pH 7.4) containing a cocktail of
367 protease and phosphatase inhibitors (Sigma-Aldrich). Samples (10-20 µg) were analyzed by 10%
368 SDS-PAGE under denaturing conditions, followed by Western blotting, using the antibodies against
369 EGFR (clone A10, sc-373746), pY1068-EGFR (sc-377547) and secondary antibodies HRP-conjugated
370 (all from Santa Cruz Biotechnology, Inc., Texas, USA). Chemiluminescent signal (Clarity Western
371 ECL Substrate, Bio-Rad) was acquired by ChemiDoc™ Imaging System (BioRad).

372 **Real-time PCR.** Total MSC RNA isolated with the Qiagen RNeasy mini kit was treated
373 with DNase I (Qiagen, Hilden, Germany) and retrotranscribed into cDNA by iScript cDNA
374 Synthesis Kit (Bio-Rad Laboratories Inc., Hercules, CA, USA). Gene specific primers were:

375 TLR-2 (sense, 5'- CTCATTGTGCCCATTTGCTCTT -3'; antisense, 5'-
376 TCCAGTGCTTCAACCCACAAC -3'), TLR-4 (sense, 5'- GGCCATTGCTGCCAACAT -3';
377 antisense, 5'- CAACAATCACCTTTTCGGCTTTT -3'), Bax (sense, 5'-
378 AGAGGATGATTGCCGCCGT -3'; antisense, 5'- CAACCACCCTGGTCTTGGATC -3'), Bcl-2
379 (sense, 5'- TGCA.CCTGACGCCCTTCAC -3'; antisense, 5'-
380 AGACAGCCAGGAGAAATCAAACAG -3'), HPRT (sense, 5'-
381 TGACCTTGATTTATTTTGCATACC -3'; antisense, 5'- CGCTTTCCATGTGTGAGGTGATG -
382 3'), RPL13A (sense, 5'-CATAGGAAGCTGGGAGCAAG-3'; antisense, 5'-
383 GCCCTCCAATCAGTCTTCTG-3'). For EGFR, NOD1 and NOD2, validated primers from Bio-
384 Rad were used (Unique Assay ID qHsaCID0007564, qHsaCED0005079 and qHsaCED0056944
385 respectively). For quantitative real-time PCR, the iQTM SYBR Green Supermix (Bio-Rad
386 Laboratories Inc., Segrate, MI, Italy) was used according to the manufacturer's instructions.
387 Reactions were run in duplicate on a CFX96 Real Time System and analyzed by BioRad CFX
388 Maestro Software (Bio-Rad Laboratories Inc.). Gene expression was normalized to HPRT or

389 RPL13A mRNA content.

390 **MTT assay.** MSC cell viability was measured by MTT 3-(4,5-dimethylthiazol-2-yl)-2,5-
391 diphenyltetrazolium bromide assay (Sigma Aldrich, MO, USA). Cells were seeded at a density of
392 2×10^3 /well in 96-well plates. After 24 h of incubation in RPMI 10% FBS without antibiotics, cells
393 were infected with *B. henselae* (MOI 100). The medium was changed after 4 days to wash out all
394 extracellular bacteria. When indicated, cells were treated with heat-killed *B. henselae*. Cells were
395 then incubated for 3 h with 20 μ l MTT (final concentration 0,5 mg/ml). Formazan crystals were
396 solubilized for 10 min in 100 μ l DMSO, and OD 570 nm was measured using a microplate reader
397 (VICTOR3TM, PerkinElmer, MA, USA). To determine the contribution of bacteria in MTT
398 reduction to overall values of infected MSCs, a bacterial suspension with the same concentrations
399 per milliliter of those recovered from cells was assessed in parallel and the obtained values
400 subtracted to results from infected cells.

401 **Annexin V Assay.** MSCs untreated or infected for 96 h with *B. henselae* were stained with
402 annexin V-FITC and PI (Sigma Aldrich) according to the manufacturer's instructions. Samples
403 were analyzed by FACS Calibur (Becton Dickinson), and results were quantified using FlowLogic
404 (Miltenyi Biotec, Bergisch Gladbach, Germany).

405 **Flow cytometry.** MSCs were collected at the indicated times after infection and
406 preincubated for 30 min at 4°C in 1X PBS supplemented with 2% goat serum and 0.2% sodium
407 azide, washed twice with 1% bovine serum albumin (BSA). Successively, cells were incubated for
408 30 min at 4°C with anti-human TLR-2 FITC (mouse IgG2a) and anti-human TLR-4 PE (mouse
409 IgG2a) or respective isotype controls (all from BioLegend CA, USA). Flow cytometry analysis was
410 performed using FACS Calibur and FlowLogic as described above.

411 **Cytokine measurements.** MSCs seeded in 24-well plates were infected with a MOI of 100
412 for the indicated times. For some experiments, cells were pretreated with the pharmacological
413 inhibitors gefitinib and GSK583 or the neutralizing antibody anti-TLR2 (anti-human TLR2-IgA,
414 clone B4H2) and the human IgA2 isotype control (both purchased from InvivoGen, CA, USA).

415 Cell-free supernatants were then harvested to measure human VEGF-A, CXCL8, IL-6 and CCL5
416 production by ELISA (R&D Systems, Minneapolis, MN, USA). To quantify human PDGF-D, a
417 specific kit from Elabscience (Wuhan, Hubei, P.R.C) was employed.

418 **Angiogenesis array.** The human angiogenesis array (Proteome Profiler™ Array; R&D
419 Systems) was used to assess the expression of 55 angiogenic-related proteins in MSCs uninfected or
420 infected with *B. henselae* for 96 h. The array membranes were probed with pooled supernatants
421 derived from three independent experiments according to manufacturer's instructions.
422 Chemiluminescent signal was acquired by ChemiDoc™ Imaging System (BioRad).
423 The signal intensity of each antigen-specific antibody spot was quantified using Fiji-ImageJ (NIH)
424 software. For comparison of the relative expression of proteins in uninfected vs infected cells, the
425 mean pixel density of the pair of duplicate spots for each protein, after subtraction of the mean pixel
426 density of the negative control spots of the respective array, was normalized to the mean pixel
427 density of the positive control spots. Heat map analysis using the normalized data was performed by
428 GraphPad PRISM 8.0 software.

429 **Sprouting assay.** Sprouting of HUVEC spheroids was assessed as described previously
430 (59). Briefly, spheroids were prepared in 20% methylcellulose medium, embedded in a fibrin gel
431 and stimulated with recombinant human VEGF-A₁₆₅ (30 ng/mL) (R&D System, MN, USA) or with
432 different concentrations of CM from uninfected or infected MSCs. The number of radially growing
433 cell sprouts was counted after 24 h using an Axiovert 200M microscope equipped with LD A Plan
434 20X/0.30PH1 objective (Carl Zeiss) and expressed as relative increase over untreated spheroids.

435 **Motility assay.** HUVEC motility assay was based on "scratch" wounding of a confluent
436 monolayer. Briefly, HUVECs (1×10^5) were seeded onto 0.1 % collagen type I (BD Biosciences,
437 Italy)-coated six-well plates in complete medium until a confluent monolayer was formed. The cell
438 monolayers were scratched using a pipette tip, washed with 1X PBS to remove the undetached cells
439 and treated with MSC conditioned medium. After 24 h, cells were photographed under an Axiovert
440 200M microscope (Carl Zeiss) equipped with LD A Plan 20X/0.30PH1. The healed area was

441 quantified through computerized analysis by subtracting the wound area at 24 h from the initial
442 area.

443 **Tube formation assay.** EC vessel formation was assessed by tube morphogenesis assay in a
444 three-dimensional (3D) collagen matrix. To this end, HUVECs were seeded onto Reduced Growth
445 Factor Basement Membrane Matrix Cultrex[®] (BME) (Trevigen, Italy)-coated μ -slide angiogenesis
446 chamber (Ibidi, Martinsried, Germany) at a density of 4.0×10^4 cells/cm² in the absence or presence
447 of CM from untreated or infected MSCs. After 48 h, cells were photographed using an Axiovert
448 200M microscope, and the number of meshes/field was counted. **Statistical Analysis.** Statistical
449 significance was determined by non-parametric Student's t-test and one-way analysis of variance
450 followed by Tukey's multiple-comparison test. Results were analyzed by GraphPad PRISM 8.0
451 software (CA, USA).

452

453 **Abbreviations**

454 MSCs: mesenchymal stromal cells

455 ECs: endothelial cells

456 DCs: dendritic cells

457 TLRs: Toll-like receptors

458 NLRs: NOD-like receptors

459 PRRs: Pattern Recognition Receptors

460 CSD: cat scratch disease

461 BA: bacillary angiomatosis

462 BP: bacillary peliosis

463 GPA: gentamicin protection assay

464 CM: conditioned medium

465 MOI: multiplicity of infection

466 BM: bone marrow

467 ANOVA: analysis of variance

468

469 **Acknowledgments**

470 The authors thank Prof William Vermi, Department of Molecular and Translational Medicine,

471 University of Brescia, for immunohistochemistry analysis of the MSC/*B. henselae* interaction.

472

473 **DECLARATIONS**

474 **Funding**

475 This work was supported by funds from the Compagnia di San Paolo, Fondazione Ricerca

476 Molinette, AIRC (Associazione Italiana Ricerca sul Cancro) project IG15811 (2015–2017), project

477 IG 20776 (2017) and project IG17276, E.G. was also supported by FUV Fellowship.

478 **Conflict of Interest Statement**

479 The authors declare that the research was conducted in the absence of any commercial or financial

480 relationships that could be construed as a potential conflict of interest.

481 **Ethics Statement**

482 This study was carried out in accordance with the recommendations of “Comitato Etico

483 Interaziendale A.O.U. Città della Salute e della Scienza di Torino—A.O. Ordine Mauriziano—ASL

484 TO1, number 0009806” with written informed consent from all subjects. All subjects gave written

485 informed consent in accordance with the Declaration of Helsinki. The protocol was approved by the

486 “Comitato Etico Interaziendale A.O.U. Città della Salute e della Scienza di Torino—A.O. Ordine

487 Mauriziano—ASL TO1.”

488 **Availability of data and materials**

489 All data and materials are available upon request.

490 **Author Contributions**

491 SaS, SM, SiS, and TM participated in the design of the study.

492 SaS, RS, GP, EG, MB, VS, DA, and TS participated in data acquisition and analysis.

493 TM, SM and SaS wrote the manuscript.

494 SiS participated in data interpretation and manuscript revision.

495

496

497

498

499 REFERENCES

500 1. Florin TA, Zaoutis TE, Zaoutis LB. 2008. Beyond Cat Scratch Disease: Widening Spectrum of *Bartonella*
501 *henselae* Infection. *Pediatrics* 121:e1413–e1425.

502 2. Harms A, Dehio C. 2012. Intruders below the Radar: Molecular Pathogenesis of *Bartonella* spp. *Clin*
503 *Microbiol Rev* 25:42–78.

504 3. McCord AM, Burgess AWO, Whaley MJ, Anderson BE. 2005. Interaction of *Bartonella henselae* with
505 Endothelial Cells Promotes Monocyte/Macrophage Chemoattractant Protein 1 Gene Expression and
506 Protein Production and Triggers Monocyte Migration. *Infect Immun* 73:5735–5742.

507 4. Berrich M, Kieda C, Grillon C, Monteil M, Lamerant N, Gavard J, Boulouis HJ, Haddad N. 2011.
508 Differential Effects of *Bartonella henselae* on Human and Feline Macro- and Micro-Vascular
509 Endothelial Cells. *PLoS ONE* 6:e20204.

510 5. Tsukamoto K, Shinzawa N, Kawai A, Suzuki M, Kidoya H, Takakura N, Yamaguchi H, Kameyama T,
511 Inagaki H, Kurahashi H, Horiguchi Y, Doi Y. 2020. The *Bartonella* autotransporter BafA activates the
512 host VEGF pathway to drive angiogenesis. *Nat Commun* 11:3571.

513 6. Musso T, Badolato R, Ravarino D, Stornello S, Panzanelli P, Merlino C, Savoia D, Cavallo R, Ponzi AN,
514 Zucca M. 2001. Interaction of *Bartonella henselae* with the Murine Macrophage Cell Line J774:
515 Infection and Proinflammatory Response. *Infect Immun* 69:5974–5980.

- 516 7. Resto-Ruiz SI, Schmiederer M, Sweger D, Newton C, Klein TW, Friedman H, Anderson BE. 2002.
517 Induction of a Potential Paracrine Angiogenic Loop between Human THP-1 Macrophages and Human
518 Microvascular Endothelial Cells during *Bartonella henselae* Infection. *Infect Immun* 70:4564–4570.
- 519 8. Mändle T, Einsele H, Schaller M, Neumann D, Vogel W, Autenrieth IB, Kempf VAJ. 2005. Infection of
520 human CD34+ progenitor cells with *Bartonella henselae* results in intraerythrocytic presence of B
521 *henselae*. *Blood* 106:1215–1222.
- 522 9. Pittenger MF, Discher DE, Péault BM, Phinney DG, Hare JM, Caplan AI. 2019. Mesenchymal stem cell
523 perspective: cell biology to clinical progress. *Npj Regen Med* 4:22.
- 524 10. Melchiorri AJ, Nguyen B-NB, Fisher JP. 2014. Mesenchymal Stem Cells: Roles and Relationships in
525 Vascularization. *Tissue Eng Part B Rev* 20:218–228.
- 526 11. Di Somma M, Schaafsma W, Grillo E, Vliora M, Dakou E, Corsini M, Ravelli C, Ronca R, Sakellariou P,
527 Vanparijs J, Castro B, Mitola S. 2019. Natural Histogel-Based Bio-Scaffolds for Sustaining Angiogenesis
528 in Beige Adipose Tissue. *Cells* 8:1457.
- 529 12. Alcayaga-Miranda F, Cuenca J, Khoury M. 2017. Antimicrobial Activity of Mesenchymal Stem Cells:
530 Current Status and New Perspectives of Antimicrobial Peptide-Based Therapies. *Front Immunol* 8.
- 531 13. Bessède E, Dubus P, Mégraud F, Varon C. 2015. *Helicobacter pylori* infection and stem cells at the
532 origin of gastric cancer. *Oncogene* 34:2547–2555.
- 533 14. De Luca A, Gallo M, Aldinucci D, Ribatti D, Lamura L, D'Alessio A, De Filippi R, Pinto A, Normanno N.
534 2011. Role of the EGFR ligand/receptor system in the secretion of angiogenic factors in mesenchymal
535 stem cells. *J Cell Physiol* 226:2131–2138.
- 536 15. Das B, Kashino SS, Pulu I, Kalita D, Swami V, Yeger H, Felsner DW, Campos-Neto A. 2013. CD271+ Bone
537 Marrow Mesenchymal Stem Cells May Provide a Niche for Dormant *Mycobacterium tuberculosis*. *Sci*
538 *Transl Med* 5:170ra13-170ra13.

- 539 16. Fatima S, Kamble SS, Dwivedi VP, Bhattacharya D, Kumar S, Ranganathan A, Van Kaer L, Mohanty S,
540 Das G. 2019. Mycobacterium tuberculosis programs mesenchymal stem cells to establish dormancy
541 and persistence. *J Clin Invest* 130:655–661.
- 542 17. Oviedo-Boyso J, Bravo-Patiño A, Baizabal-Aguirre VM. 2014. Collaborative Action of Toll-Like and Nod-
543 Like Receptors as Modulators of the Inflammatory Response to Pathogenic Bacteria. *Mediators*
544 *Inflamm* 2014:1–16.
- 545 18. Ho J, Moyes DL, Tavassoli M, Naglik JR. 2017. The Role of ErbB Receptors in Infection. *Trends*
546 *Microbiol* 25:942–952.
- 547 19. Koff JL, Shao MXG, Ueki IF, Nadel JA. 2008. Multiple TLRs activate EGFR via a signaling cascade to
548 produce innate immune responses in airway epithelium. *Am J Physiol-Lung Cell Mol Physiol*
549 294:L1068–L1075.
- 550 20. McCord AM, Resto-Ruiz SI, Anderson BE. 2006. Autocrine Role for Interleukin-8 in *Bartonella*
551 *henselae*-Induced Angiogenesis. *Infect Immun* 74:5185–5190.
- 552 21. Rezaie J, Heidarzadeh M, Hassanpour M, Amini H, Shokrollahi E, Ahmadi M, Rahbarghazi R. 2020. The
553 Angiogenic Paracrine Potential of Mesenchymal Stem Cells, p. . *In* Ahmed Al-Anazi, K (ed.), Update on
554 Mesenchymal and Induced Pluripotent Stem Cells. IntechOpen.
- 555 22. Nassiri SM, Rahbarghazi R. 2013. Interactions of Mesenchymal Stem Cells with Endothelial Cells. *Stem*
556 *Cells Dev* 23:319–332.
- 557 23. Kempf VA, Volkmann B, Schaller M, Sander CA, Alitalo K, Riess T, Autenrieth IB. 2001. Evidence of a
558 leading role for VEGF in *Bartonella henselae*-induced endothelial cell proliferations. *Cell Microbiol*
559 3:623–632.
- 560 24. Dehio C. 2005. *Bartonella* –host-cell interactions and vascular tumour formation. 8. *Nat Rev Microbiol*
561 3:621–631.

- 562 25. Vermi W. 2006. Role of dendritic cell-derived CXCL13 in the pathogenesis of *Bartonella henselae* B-
563 rich granuloma. *Blood* 107:454–462.
- 564 26. Kempf VAJ, Schaller M, Behrendt S, Volkmann B, Aepfelbacher M, Cakman I, Autenrieth IB. 2000.
565 Interaction of *Bartonella henselae* with endothelial cells results in rapid bacterial rRNA synthesis and
566 replication. *Cell Microbiol* 2:431–441.
- 567 27. Kempf VAJ, Schairer A, Neumann D, Grassl GA, Lauber K, Lebidziejewski M, Schaller M, Kyme P,
568 Wesselborg S, Autenrieth IB. 2005. *Bartonella henselae* inhibits apoptosis in Mono Mac 6 cells: *B.*
569 *henselae* inhibits apoptosis in monocytes. *Cell Microbiol* 7:91–104.
- 570 28. Truttmann MC, Misselwitz B, Huser S, Hardt W-D, Critchley DR, Dehio C. 2011. *Bartonella henselae*
571 engages inside-out and outside-in signaling by integrin β 1 and talin1 during invasome-mediated
572 bacterial uptake. *J Cell Sci* 124:3591–3602.
- 573 29. Najar M, Krayem M, Meuleman N, Bron D, Lagneaux L. 2017. Mesenchymal Stromal Cells and Toll-Like
574 Receptor Priming: A Critical Review. *Immune Netw* 17:89.
- 575 30. Strober W, Murray PJ, Kitani A, Watanabe T. 2006. Signalling pathways and molecular interactions of
576 NOD1 and NOD2. *Nat Rev Immunol* 6:9–20.
- 577 31. Haile PA, Votta BJ, Marquis RW, Bury MJ, Mehlmann JF, Singhaus R, Charnley AK, Lakdawala AS,
578 Convery MA, Lipshutz DB, Desai BM, Swift B, Capriotti CA, Berger SB, Mahajan MK, Reilly MA, Rivera
579 EJ, Sun HH, Nagilla R, Beal AM, Finger JN, Cook MN, King BW, Ouellette MT, Totoritis RD,
580 Pierdomenico M, Negroni A, Stronati L, Cucchiara S, Ziłkowski B, Vossenkämper A, MacDonald TT,
581 Gough PJ, Bertin J, Casillas LN. 2016. The Identification and Pharmacological Characterization of 6-(
582 *tert*-Butylsulfonyl)-*N*-(5-fluoro-1*H*-indazol-3-yl)quinolin-4-amine (GSK583), a Highly Potent and
583 Selective Inhibitor of RIP2 Kinase. *J Med Chem* 59:4867–4880.

- 584 32. Viala J, Chaput C, Boneca IG, Cardona A, Girardin SE, Moran AP, Athman R, Mémet S, Huerre MR,
585 Coyle AJ, DiStefano PS, Sansonetti PJ, Labigne A, Bertin J, Philpott DJ, Ferrero RL. 2004. Nod1 responds
586 to peptidoglycan delivered by the *Helicobacter pylori* cag pathogenicity island. *Nat Immunol* 5:1166–
587 1174.
- 588 33. Kim JG, Lee SJ, Kagnoff MF. 2004. Nod1 Is an Essential Signal Transducer in Intestinal Epithelial Cells
589 Infected with Bacteria That Avoid Recognition by Toll-Like Receptors. *Infect Immun* 72:1487–1495.
- 590 34. Opitz B, Förster S, Hocke AC, Maass M, Schmeck B, Hippenstiel S, Suttorp N, Krüll M. 2005. Nod1-
591 Mediated Endothelial Cell Activation by *Chlamydomphila pneumoniae*. *Circ Res* 96:319–326.
- 592 35. Tigno-Aranjuez JT, Asara JM, Abbott DW. 2010. Inhibition of RIP2's tyrosine kinase activity limits
593 NOD2-driven cytokine responses. *Genes Dev* 24:2666–2677.
- 594 36. Duran A, Valero N, Mosquera J, Fuenmayor E, Alvarez-Mon M. 2017. Gefitinib and pyrrolidine
595 dithiocarbamate decrease viral replication and cytokine production in dengue virus infected human
596 monocyte cultures. *Life Sci* 191:180–185.
- 597 37. Bentz GL, Yurochko AD. 2008. Human CMV infection of endothelial cells induces an angiogenic
598 response through viral binding to EGF receptor and β 1 and β 3 integrins. *Proc Natl Acad Sci* 105:5531–
599 5536.
- 600 38. Singh B, Carpenter G, Coffey RJ. 2016. EGF receptor ligands: recent advances. *F1000Research* 5:2270.
- 601 39. Swanson KV, Griffiss JM, Edwards VL, Stein DC, Song W. 2011. *Neisseria gonorrhoeae*-induced
602 transactivation of EGFR enhances gonococcal invasion. *Cell Microbiol* 13:1078–1090.
- 603 40. Keates S, Keates AC, Katchar K, Peek, Jr. RM, Kelly CP. 2007. *Helicobacter pylori* Induces Up-Regulation
604 of the Epidermal Growth Factor Receptor in AGS Gastric Epithelial Cells. *J Infect Dis* 196:95–103.

- 605 41. Zhang J, Li H, Wang J, Dong Z, Mian S, Yu F-SX. 2004. Role of EGFR Transactivation in Preventing
606 Apoptosis in *Pseudomonas aeruginosa*-Infected Human Corneal Epithelial Cells. *Invest Ophthalmol*
607 *Vis Sci* 45:2569–2576.
- 608 42. Yan F, Cao H, Chaturvedi R, Krishna U, Hobbs SS, Dempsey PJ, Peek RM, Cover TL, Washington MK,
609 Wilson KT, Polk DB. 2009. Epidermal growth factor receptor activation protects gastric epithelial cells
610 from *Helicobacter pylori*-induced apoptosis. *Gastroenterology* 136:1297–1307, e1-3.
- 611 43. Brandau S, Jakob M, Bruderek K, Bootz F, Giebel B, Radtke S, Mauel K, Jäger M, Flohé SB, Lang S. 2014.
612 Mesenchymal Stem Cells Augment the Anti-Bacterial Activity of Neutrophil Granulocytes. *PLOS ONE*
613 9:e106903.
- 614 44. Chandra PK, Gerlach SL, Wu C, Khurana N, Swintoniewski LT, Abdel-Mageed AB, Li J, Braun SE,
615 Mondal D. 2018. Mesenchymal stem cells are attracted to latent HIV-1-infected cells and enable virus
616 reactivation via a non-canonical PI3K-NFκB signaling pathway. *Sci Rep* 8:14702.
- 617 45. O'Rourke F, Mändle T, Urbich C, Dimmeler S, Michaelis UR, Brandes RP, Flötenmeyer M, Döring C,
618 Hansmann M-L, Lauber K, Ballhorn W, Kempf VAJ. 2015. Reprogramming of myeloid angiogenic cells
619 by *Bartonella henselae* leads to microenvironmental regulation of pathological angiogenesis. *Cell*
620 *Microbiol* 17:1447–1463.
- 621 46. Kempf VAJ, Hitziger N, Riess T, Autenrieth IB. 2002. Do plant and human pathogens have a common
622 pathogenicity strategy? *Trends Microbiol* 10:269–275.
- 623 47. Del Prete A, Scutera S, Sozzani S, Musso T. 2019. Role of osteopontin in dendritic cell shaping of
624 immune responses. *Cytokine Growth Factor Rev* 50:19–28.
- 625 48. Raghuvanshi S, Sharma P, Singh S, Van Kaer L, Das G. 2010. *Mycobacterium tuberculosis* evades host
626 immunity by recruiting mesenchymal stem cells. *Proc Natl Acad Sci* 107:21653–21658.

- 627 49. Dehghani Nazhvani A, Ahzan S, Hosseini S-M, Attar A, Monabati A, Tavangar MS. 2018. Purification of
628 Stem Cells from Oral Pyogenic Granuloma Tissue. *Open Dent J* 12:560–566.
- 629 50. Scutera S, Salvi V, Lorenzi L, Piersigilli G, Lonardi S, Alotto D, Casarin S, Castagnoli C, Dander E,
630 D’Amico G, Sozzani S, Musso T. 2018. Adaptive Regulation of Osteopontin Production by Dendritic
631 Cells Through the Bidirectional Interaction With Mesenchymal Stromal Cells. *Front Immunol* 9:1207.
- 632 51. Mitroulis I, Kalafati L, Bornhäuser M, Hajishengallis G, Chavakis T. 2020. Regulation of the Bone
633 Marrow Niche by Inflammation. *Front Immunol* 11.
- 634 52. Tamma R, Ribatti D. 2017. Bone Niches, Hematopoietic Stem Cells, and Vessel Formation. *Int J Mol Sci*
635 18.
- 636 53. Perucca S, Di Palma A, Piccaluga PP, Gemelli C, Zoratti E, Bassi G, Giacomuzzi E, Lojacono A, Borsani G,
637 Tagliafico E, Scupoli MT, Bernardi S, Zanaglio C, Cattina F, Cancelli V, Malagola M, Krampera M, Marini
638 M, Almici C, Ferrari S, Russo D. 2017. Mesenchymal stromal cells (MSCs) induce ex vivo proliferation
639 and erythroid commitment of cord blood haematopoietic stem cells (CB-CD34+ cells). *PLoS One*
640 12:e0172430.
- 641 54. Hipp SJ, Shields A, Fordham LA, Blatt J, Hamrick HJ, Henderson FW. 2005. Multifocal Bone Marrow
642 Involvement in Cat-Scratch Disease: *Pediatr Infect Dis J* 24:472–474.
- 643 55. Donà D, Nai Fovino L, Mozzo E, Cabrelle G, Bordin G, Lundin R, Giaquinto C, Zangardi T, Rampon O.
644 2018. Osteomyelitis in Cat-Scratch Disease: A Never-Ending Dilemma—A Case Report and Literature
645 Review. *Case Rep Pediatr* 2018:1–8.
- 646 56. Randell MG, Balakrishnan N, Gunn-Christie R, Mackin A, Breitschwerdt EB. 2018. *Bartonella henselae*
647 infection in a dog with recalcitrant ineffective erythropoiesis. *Vet Clin Pathol* 47:45–50.

- 648 57. Riess T, Dietrich F, Schmidt KV, Kaiser PO, Schwarz H, Schäfer A, Kempf VAJ. 2008. Analysis of a Novel
649 Insect Cell Culture Medium-Based Growth Medium for Bartonella Species. Appl Environ Microbiol
650 74:5224–5227.
- 651 58. Rolain JM, La Scola B, Liang Z, Davoust B, Raoult D. 2001. Immunofluorescent detection of
652 intraerythrocytic Bartonella henselae in naturally infected cats. J Clin Microbiol 39:2978–2980.
- 653 59. Rezzola S, Di Somma M, Corsini M, Leali D, Ravelli C, Polli VAB, Grillo E, Presta M, Mitola S. 2019.
654 VEGFR2 activation mediates the pro-angiogenic activity of BMP4. Angiogenesis 22:521–533.

655

656

657

658 **FIGURE LEGENDS**

659

660 **FIG. 1 *B. henselae* invades and persists in MSCs.** (a) Invasion rates of *B. henselae* into MSCs
661 were measured at day 1, 2, 3, 4 and 8 pi by gentamicin protection assay (GPA). After infection,
662 cells were treated with gentamicin, and the number of intracellular bacteria was determined by CFU
663 count. Data are expressed as mean \pm SEM from two independent experiments carried out in
664 triplicate ($*P < 0.05$ vs Log₁₀ CFU at 1 day; unpaired t-test). (b) Uninfected (CTRL) or *B. henselae*-
665 infected MSCs (8 days) were immunostained with an anti-BH antibody and counterstained with
666 hematoxylin (upper panel 20X, lower panel 40X) or with goat anti-mouse Alexa Fluor® 594
667 conjugate and DAPI for immunofluorescence visualization (lower panel 100X). (c) To determine
668 intracellular survival after 4 days of infection, extracellular bacteria were killed by gentamicin
669 treatment and incubated in normal medium for the indicated times. Mean values \pm SEM of four
670 independent experiments performed in triplicate ($*P < 0.05$; unpaired t-test). (d) Invasion rates of *B.*
671 *henselae* in MSCs or HUVECs (60,000 cells each, respectively). The number of intracellular

672 bacteria as Log₁₀ CFU was quantified at 1 day pi. Mean ± SEM of three experiments (**P* < 0.05
673 MSCs vs HUVECs; unpaired t-test).

674 **FIG. 2 *B. henselae* localizes in invasome structures in MSCs.** (a) Immunofluorescence of *B.*
675 *henselae*-infected MSCs at 1, 2, 4 and 8 days pi and uninfected control MSCs (CTRL). *B. henselae*
676 and cell membranes were stained with DAPI (cyan) and wheat germ agglutinin-Alexa Fluor 594
677 (red), respectively, and analyzed with an epifluorescence microscope. Bacteria anchored to the
678 MSC membrane are indicated with arrowheads. The thin arrows (2 and 4 days) indicate internalized
679 bacteria within membrane bound compartments in the perinuclear area, whereas the large arrows (8
680 days) highlight sizeable intracellular bacterial aggregates called invasomes. Each image also shows
681 the basal portion of adherent MSC cells, with the orthogonal *z* reconstruction of the whole cell. (b)
682 Representative image of an invasome. MSCs were infected with *B. henselae* for 8 days and then
683 washed and fixed with PFA. Samples were stained for F-actin (red), wheat germ agglutinin (WGA)
684 (green) and DAPI and analyzed as described in panel a (bar: 10 μm).

685 **FIG. 3 *B. henselae* favors the proliferation of infected MSCs.** (a) MSC death was evaluated by
686 FACS analysis after 4 days of infection with *B. henselae*. Uninfected MSCs (left panel; CTRL) and
687 infected MSCs (right panel; *B. henselae*) were double-stained with FITC-annexin V and PI.
688 Counterstaining with PI allowed differentiation of necrotic cells (upper left quadrant of the dot
689 plot), late apoptotic cells (upper right quadrant) and early apoptotic cells (lower right quadrant). The
690 percentages of cells localizing to these quadrants are indicated in each quadrant. Data are
691 representative of three independent experiments. (b) The Bcl-2/Bax expression ratio was analyzed
692 in control and *B. henselae*-infected MSCs at 2 days pi by qPCR. Gene expression was normalized
693 to HPRT. Data are expressed as mean ± SEM of four independent experiments (ns not significant;
694 unpaired t-test). (c) Proliferation assay. MSCs were treated as indicated for 0, 2, 4, and 8 days and
695 analyzed by MTT assay. Untreated MSCs (white circle); *B. henselae* infected MSC (black circle);
696 and heat killed *B. henselae*-treated MSCs (HK *B.henselae*) (grey circle). Data are expressed as

697 mean \pm SEM of three independent experiments performed in triplicate ($*P < 0.05$ *B. henselae* vs
698 CTRL, unpaired t-test).

699 **FIG. 4 Expression of TLR2, NOD1 and EGFR in *B. henselae*-infected MSCs.** (a) mRNA
700 expression levels of TLR2, TLR4, NOD1 and EGFR in uninfected (white bar) and *B. henselae*-
701 infected MSCs (black bar) were determined by qPCR and normalized to RPL13A. Data are
702 expressed as mean \pm SEM of four independent experiments ($* P < 0.05$; unpaired t-test). (b) TLR2
703 and TLR4 protein expression levels on MSC membranes were analyzed by FACS in MSCs at 4
704 days pi. Cells were immunostained with anti-TLR2, anti-TLR4 or specific isotype control
705 antibodies. The percentages of positive cells are indicated in each quadrant. Fluorescence minus one
706 (FMO) controls for the antibodies are shown as well. Data are representative of three independent
707 experiments (left panel) or as mean \pm SEM (right panel). (c) Cell extracts from MSCs infected with
708 *B. henselae* for 30, 60, and 120 min or with hEGF (50 ng/mL) for 15 min were subjected to
709 immunoblotting using anti-EGFR pY1068 or anti-EGFR antibodies. (d) Analysis of CXCL8 in the
710 supernatants from uninfected or *B. henselae*-infected MSCs pre-treated or not for 6 h with a
711 neutralizing anti-TLR2 antibody (10 μ g/mL) (upper panel, n=6 experiments) or with the EGFR
712 inhibitor gefitinib (10 μ M) or the RIP2K inhibitor GSK583 (1 μ M) (lower panel, n= 4 experiments)
713 and then stimulated for 96 h. Data are shown as percentage (means \pm SEM) of CXCL8 production
714 compared to specific isotype control antibody or DMSO respectively set as 100% ($* P < 0.05$ vs *B.*
715 *henselae*-infected cells; unpaired t-test). (e) To evaluate *B. henselae* internalization, MSCs were
716 pretreated for 6 h with the neutralizing anti-EGFR (10 μ g/mL) (upper panel, n=3 independent
717 experiments) or gefitinib (10 μ M) (lower panel, n=4 independent experiments), and CFU values of
718 intracellular bacteria, determined, after 1 and 2 days of incubation, are expressed as percentage
719 relative to CFU of specific isotype control antibody or DMSO-treated cells set as 100%. Data are
720 shown as mean \pm SEM; $* P < 0.05$ vs internalized bacteria in untreated cells; unpaired t-test.

721 **FIG. 5 Conditioned medium from *B. henselae*-infected MSCs curbs the infection rates and**
722 **angiogenic response of HUVECs.** The effects of conditioned medium (CM) from *B. henselae*-
723 infected MSCs were tested by means of different angiogenic assays. (a) HUVEC monolayers were
724 wounded with a 1.0-mm-wide rubber policeman and incubated in fresh medium supplemented with
725 5% FCS and 1:2 diluted CM from infected (black bar, CM-MSC CTRL) or uninfected (white bar,
726 CM-MSC *B. henselae*) MSCs. After 1 day, HUVECs invading the wound were quantified by
727 digital imaging to calculate the relative increment in cell-covered area induced by MSC-CM
728 compared to untreated HUVECs. Mean \pm SEM of three independent experiments. * $P < 0.05$ vs Ctrl;
729 unpaired t-test. (b) Sprouting analysis of HUVEC spheroids. Spheroids were prepared in 20%
730 methylcellulose medium, embedded in fibrin gel and stimulated with 1:2 diluted CM obtained from
731 MSCs treated in the presence (black bar) or absence (white bar) of bacteria or with 30 ng/ml VEGF-
732 A (dashed bar). The number of growing cell sprouts was counted after 1 day. Data are expressed as
733 mean fold change vs Ctrl \pm SEM of 20-40 spheroids/ experimental condition in three independent
734 experiments and indicated as fold increase in the number of sprouts/spheroid vs Ctrl. * $P < 0.05$ vs
735 Ctrl; unpaired t-test. (c) The effect of CM from uninfected vs *B. henselae*-infected MSCs on
736 HUVEC morphogenesis was assessed by tube morphogenesis assay in three-dimensional (3D)
737 collagen matrix. HUVECs were seeded (40000 cells/cm²) on Cultrex Extracellular Matrix in the
738 presence of 1:2 diluted CM from uninfected (white bar) or *B. henselae*-infected MSCs (black bar).
739 After 8 h, the formation of capillary-like structures was examined. Representative images are shown
740 in the left panels. Quantification (right panel) was performed to calculate the relative increment in
741 capillary-like structure induced by MSC-CM compared to untreated HUVECs. Data are expressed
742 as mean \pm SEM relative to three independent experiments. * $P < 0.05$ vs Ctrl; unpaired t-test. (d)
743 Invasion rate of *B. henselae* in HUVECs (expressed as total CFUs) after 1 day of infection in the
744 absence (grey bar) or presence of 1:2 diluted CM-MSC CTRL (white bar) and CM-MSC *B.*
745 *henselae* (black bar). Mean \pm SEM of three independent experiments * $P < 0.05$; unpaired t-test.

746 **FIG. 6 Angiogenic signature of *B. henselae*-infected MSCs.** (a) Human angiogenesis antibody
747 array analysis was performed using a pool of supernatants from 96 h uninfected MSC (CTRL) or *B.*
748 *henselae*-infected MSCs. Some of the most representative angiogenic factors are highlighted in
749 different colors. (b) Representative heat map (left panel) and relative gene expression shown as
750 normalized pixel density of the duplicated spots for each angiogenic-related protein in the array of
751 supernatants of MSCs and *B. henselae*-infected MSCs (right panel). * P < 0.01 ** P < 0.001 vs
752 CTRL; ANOVA followed by Tukey's multiple-comparison test. (c) Quantification of VEGF-A,
753 CXCL8, IL-6, CCL5 and PDGF-D production in uninfected (CTRL) and *B. henselae*-infected
754 MSCs. Data are expressed as mean \pm SEM of three independent experiments. * P < 0.05 vs CTRL;
755 unpaired t-test. nd= not detectable.

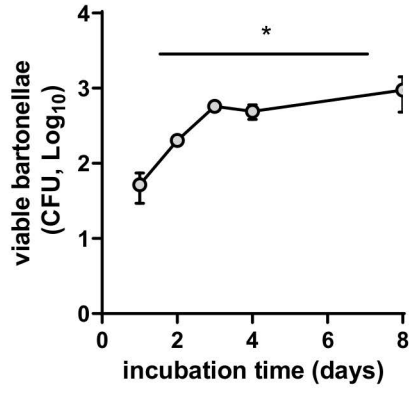
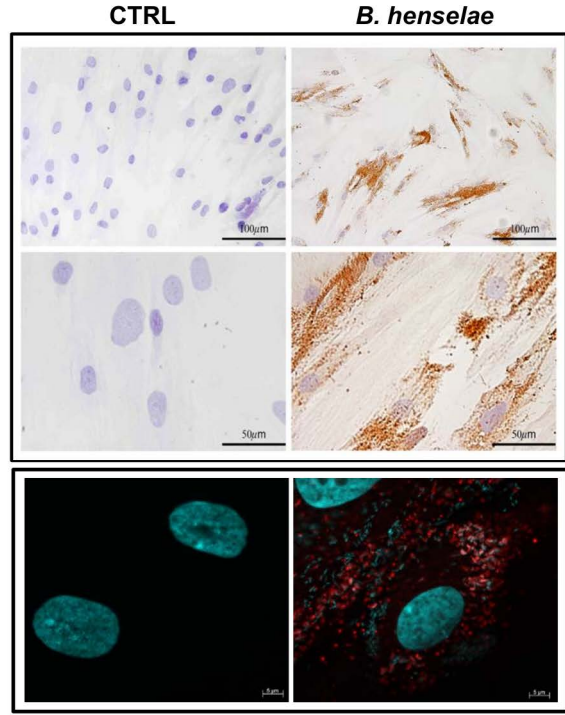
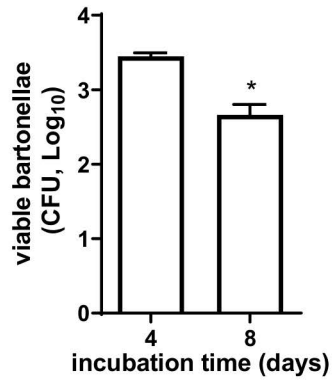
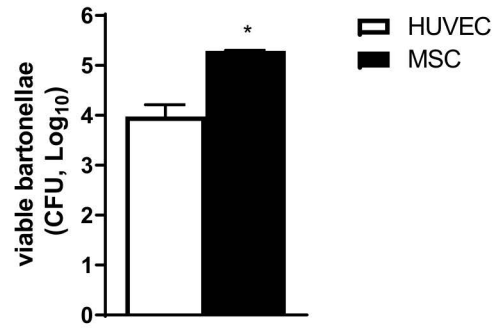
756

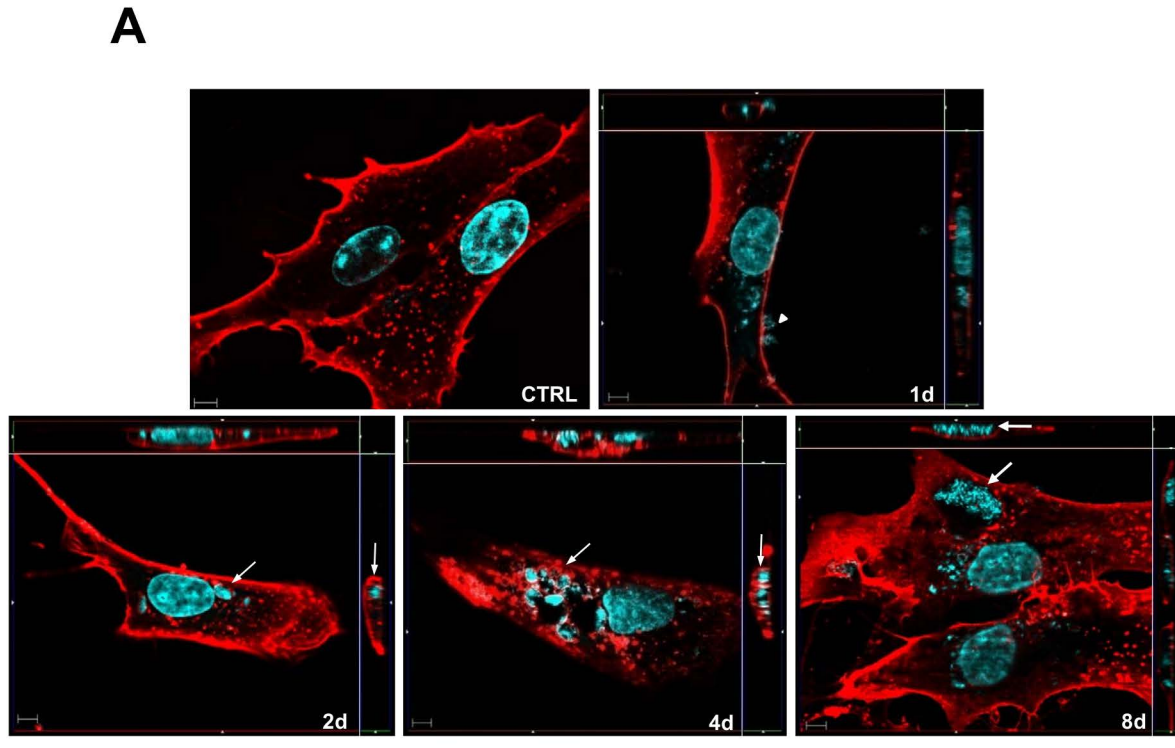
757

758

759 **Figure 1**

760

A**B****C****D**



B

